A novel induction-based device for the measurement of the complex magnetic susceptibility

Marina Díaz Michelena [a],*, Jose Luis Mesa Uña [a], Marina Pérez Jimenez [b], Marco César Maicas Ramos [b], Pedro Cobos Arribas [b], Claudio Aroca Hernández-Ros [b]

[a] Payloads and Space Sciences Dept., Instituto Nacional de Técnica Aeroespacial, Ctra. Ajalvir km.4, 28850, Torrejón de Ardoz, Spain
[b] ETSIT- ISOM, Universidad Politécnica de Madrid, Ciudad Universitaria s/n, 28040 Madrid, Spain

ARTICLE INFO

ABSTRACT

A device named magnetic susceptometer for a complete determination of the magnetic complex susceptibility of materials and minerals has been conceived and manufactured as a complement for the in situ characterization of rocks during high resolution magnetic prospections. In this work a device and its capabilities for susceptibility measurements are described, the calibration performed with artificial samples, and the values of real and imaginary susceptibility of natural samples in a range comprising: $\chi = 10^{-4}$ to 10^{-7} [SI], representative of Earth and also Mars rocks.

1. Introduction

Complex magnetic susceptibility determination of natural and synthetic samples is an important measurement for its complete magnetic characterization. Magnetic losses, eddy currents, accumulated magnetic energy, and changes on these and other properties under variations of amplitude and frequency of an external magnetic field may be of interest in the characterization of synthetic materials for some applications like transformers and superconductivity "Singh et al. [1]", and basic science like spin glasses, phases transitions and superparamagnetism characterization "Mulder et al. [2], and del Barco el al. [3]". It also can give relevant information of the conditions of formation (global magnetic fields) or cooling and alteration processes (atmospheric temperature and environmental conditions) in the study of natural rocks, where the remanent magnetization measurement is not enough to extract relevant parameters "Pandarinath [4]".

The determination of the complex susceptibility implies not only the measurement of initial susceptibility and determination of the hysteresis loop "Singh et al. [1], Mulder et al. [2], and del Barco et al. [3]", but also the behavior of the material under the action of an alternating magnetic field.

Current magnetic susceptibility measurements are performed in devices "Marcon and Ostanina [5]" based on magnetic induction like Vibrating Sample Magnetometers (VSM) "Foner [6]" or Alternating Force Magnetometers (AFM) as in Vibrating Wire Susceptometer from "Asti et al. [7]" for the real part, and magneto-optical methods "Motta et al. [8]" as well as Superconducting Quantum Interference Devices (SQUID) "Li et al. [9]" can determine the real and imaginary components. Additionally, other techniques using Micro-Electro-Mechanical Systems (MEMS) "Drung et al. [10]" or Nuclear Magnetic Resonance (NMR) "Duyn [11]" have been more recently introduced. These examples of equipment provide high-resolution susceptibility values "Mulder et al. [2]" but have high power consumption, often consist in complex procedures and are limited to medium to large laboratory facilities due to the large dimensions of the devices and maintenance resources. In all cases, very little portable equipment exists, it is considered bulky and often requires liquid nitrogen for its operation "Timofeev et al.

* Corresponding author.
E-mail address: diazma@inta.es (M. Díaz Michelena).

[12]". This is a limitation to studies, which need the analysis of natural samples because on the one hand a process of sample collection and transportation to the facility is needed, and on the other hand because the exhaustive analysis of the collected sample can lead to non-appropriate conclusions if it lacks representativeness. Furthermore, along the sequence of processes, any gap in the traceability might result in the loss of information regarding the original orientation of the samples, essential for paleomagnetic studies and with implications on the structural anisotropies.

An in situ prospection including susceptibility as well as magnetic field vector measurements is highly recommended because magnetic signatures and properties of outcrops, when measured in the nature, are the result of the contribution not only from surface rocks, but also from the magnetic properties of the subsurface and surroundings "Michelena and Kilian [13]". Therefore, complementary in situ analyses are highly desired and they suppose a very powerful tool from which many scientific and industrial sectors like Paleomagnetism, Geology, Geophysics, Mining, Oil Industry, Arqueology, etc "Clark [14] and Murdock et al. [15]" can be benefited.

The presented device has been conceived as a part of a compact and portable multisensor magnetic instrument, with the capability to measure the magnetic field and therefore an estimation of the vector (three axes): Natural Remanent Magnetization (NRM) + induced magnetization, the Magnetic Susceptibility and the minor hysteresis loops of the minerals "Day [16] and Dunlop [17]". In this work we focus on the capability of the device to measure the magnetic susceptibility, and therefore name the device susceptometer.

2. Methodology

The susceptometer is based on an inductive circuit comprising an autoinduction with an H shaped ferrite core (Fig. 1) and two capacitors connected in series and parallel with the coil (Fig. 2). The circuit is brought to the natural RLC resonance, which minimizes its power consumption. In these circumstances, along the working cycles, the capacitor C_1 (in parallel to the autoinduction) sources a high current to the coil, which generates fields in the gap of the magnetic circuit in the order of 30 mT.

When a magnetic or metallic material is approached to the bottom gap of the ferrite, the magnetic induction (B) in this part of the magnetic circuit changes, as a consequence of the different relative real permittivity (μ') of the material respect to the air (upper gap). Even more, due to the complex nature of the permeability (composed by a real: μ' and an imaginary part: μ''), other dissipation processes might be unchained in the gap, like eddy currents or processes of spin relaxation.

The change in the magnetic circuit gap induction results in a variation of the autoinductance, which can be easily measured by the corresponding change of resonance frequency of the electrical circuit. Additionally, the dissipation effects are reflected in the fields involved in the magnetic circuit as well as in a change of the voltage drop in the input resistance (R_{in}). The ferrite core has a coupled pair of secondary coils that measure the variation of the magnetic field on the two edges, when a sample is presented to one of them. The variation in the amplitude and phase of the field measured with this secondary coils corresponds with the difference between relative real and imaginary components of the susceptibility of the air and the sample.

Therefore measuring these parameters experimentally, it is possible to obtain a value of the magnetic complex relative permeability. ($\mu = \mu' + i\,\mu''$) i.e. susceptibility ($\chi = \chi' + i\,\chi'' = \mu - 1$ in the International System).

Also, the system is provided with several sets of capacitors to perform complex susceptibility measurements as a function of the frequency in the range between 10 and 100 kHz.
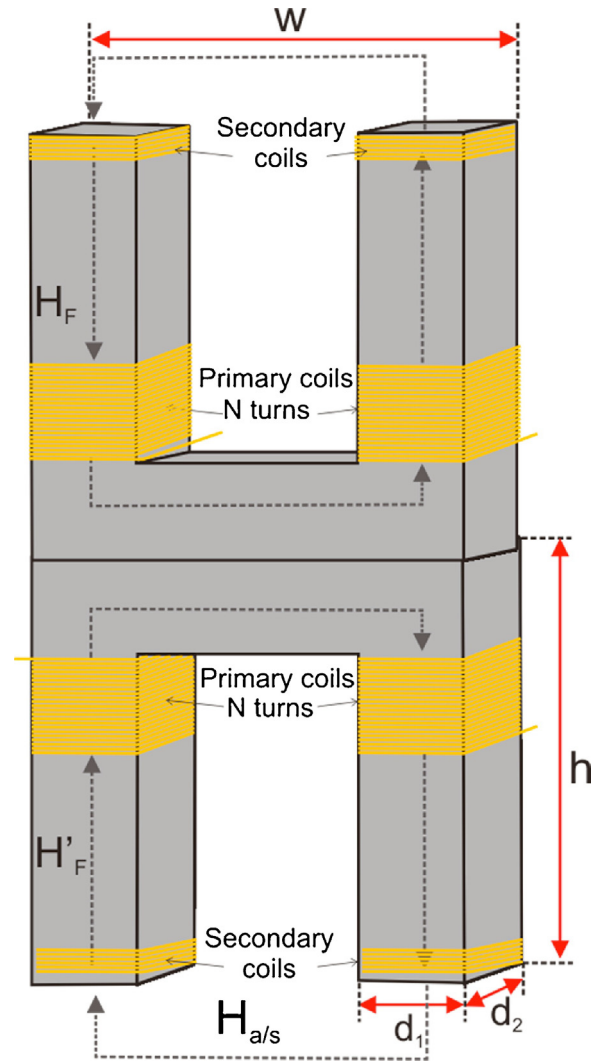

Fig. 1. Scheme of the autoinductance based on a U-shaped ferrite core. Primary coils are connected in series. Secondary coils are connected in series within every U but in opposition between the upper and lower parts of the H.
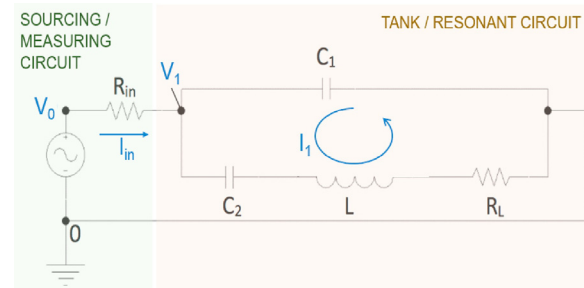

Fig. 2. Scheme of the electrical circuit. A modified tank circuit.

2.1. Mathematics

In this section we introduce the expressions to derive the real and imaginary parts of the permeability as a function of the indirect measurements performed in the electrical circuit.

The total impedance of circuit in Fig. 1 is:

$$Z_T = R_{in} + [(Z_{C_1})^{-1} + (Z_L + Z_{C_2} + R_L)^{-1}]^{-1} \qquad (1)$$

where $Z_{C_1} = \frac{1}{i\omega C_1}$, $Z_{C_2} = \frac{1}{i\omega C_2}$ and $Z_L = R_L + i\omega L$.

Table 1
Properties of the sensor head capacitors C1 and C2 and current amplification ration in the resonant circuit.

f_r (kHz) [a]	C (μF) [b]	$L \times \phi$ (mm^2) [c]	Tol. (%) [d]	Disipation [e]	I Ampl. Ratio [f]
14.21	4.700	37×27.0	± 20	$\leq 6 \times 10^{-2}$	1:06
31.42	1.000	44×20.0	± 10	$\leq 5 \times 10^{-4}$	1:12
56.80	0.330	33×17.5	± 10	$\leq 5 \times 10^{-4}$	1:37

[a] fr is the resonance frequency of the circuit.
[b] C is the capacitance of the capacitors in the sensor head resonant circuit.
[c] Dimensions of the capacitors: L is the Length and ϕ is the diameter/size.
[d] Size tolerance of the capacitance.
[e] Disipation ratio of the capacitors (dimensionless) at 1 kHz and room temperature (+ 25 °C ± 5 °C).
[f] I is electrical current. Ampl. Is Amplification. This value refers to the current through the coil achieved when 1 A passes through R_{in}.

For simplicity we assume that $C_1 = C_2 = C$, which is in agreement with the values of Table 1. The electrical circuit has two resonance states: one at $\omega_0 = \sqrt{\frac{2}{LC}}$, which minimizes the losses in the branch of the ferrite and the power consumption and another at $\omega_1 = \sqrt{\frac{1}{LC}}$, which maximizes them. The device is driven at ω_0, for which the capacitors and the autoinductance maintain a high current through the resonating branch with a relative low input current (up to I_1: $I_{in} = 37{:}1$ factors).

The real part of the susceptibility χ' is measured by the change of resonant frequency of the circuit, given the fact that the resonant frequency is directly related to the autoinductance of the electrical circuit, and this is proportional to the permeability through the reluctance of the circuit.

In the absence of a magnetic sample, the magnetic circuit is constituted by the ferrite core (indicated with the sub index "F") and an air gap (sub index "a"). In the presence of an approaching sample, the magnetic circuit is constituted by the ferrite core and the sample within the terrain (sub index "s"). In both cases, the circuit is described by:

$$\Phi R_m = NI \tag{2}$$

Φ being the magnetic flux, R_m the magnetic reluctance, N the number of turns and I the electrical current.

Therefore, the autoinductance $L = N\frac{d\Phi}{dI}$ can be calculated as $L_i = \frac{N}{R_i}$, where $R_i = \frac{l_F}{S_F}\frac{1}{\mu_F} + \frac{l_i}{S_i}\frac{1}{\mu_i}$ and the sub index "i" is associated to the air or to the terrain sample (i = a, s), which closes the magnetic circuit.

Taking this into account and due to the fact that the permeability of the air is considered μ_0, the expression of the real part of the permeability (μ'_s) and the susceptibility (χ'_s) as a function of the frequency is:

$$\mu'_s = \frac{2\pi^2 N^2 C \frac{S_F \mu_F}{l_F} f_{0,a}^2 - 1}{2\pi^2 N^2 C \frac{S_F \mu_F}{l_F} f_{0,s}^2 - 1} \tag{3}$$

and

$$\chi'_s = \frac{f_{0,a}^2 - f_{0,s}^2}{f_{0,s}^2 - \frac{l_F}{2\pi^2 N^2 C S_F \mu_F}} \tag{4}$$

where: $f_{0,a/s} = \frac{\omega_{0,a/s}}{2\pi}$, l_F is the length of the circuit in the ferrite: $l_F = 2 h + w$, $l_{a/s}$ is the length of the magnetic circuit in the air/soil $l_{a/s} = \frac{l_F}{4}$, N is the number of turns, C is the capacitors of the circuit, μ_F is the permeability of the ferrite and it has been assumed for simplicity that the ferrite and air/sample surfaces are equal: $S_F = S_a = S_s = d_1 * d_2$ (Fig. 1). The section of the ferrite is not exactly of the same dimensions of the surface comprising the field lines in the air/soil (Fig. 1). In contrast, this last one is estimated to be 3 times higher than that of the ferrite. Additionally, the air and soil surfaces will not be necessarily be the same either. This question is discussed in section V.

To measure the imaginary part of the permeability (μ'') or susceptibility (χ'') we focus on the losses of the circuit and the change of these losses in the presence of the sample.

One way to measure the imaginary susceptibility is to measure the change in voltage drop through R_{in} in the presence and absence of sample: $\Delta V(R_{in})$, because the power dissipated in this resistor $P(R_{in}) = I_{in}V(R_{in})$ is a reflection of the power loses in the resonating circuit. This method is appropriate when the imaginary part is significant. For natural samples this is not generally the case and therefore, and a method with better resolution would be preferable.

Another way to quantify the imaginary susceptibility, when the susceptibility of the ferrite is known and the real part of the susceptibility of the sample has been already determined, is to measure the magnetic field in the magnetic circuit. The magnetic induction in the ferrite bottom side in contact to the sample (B_{F-s}) is a function of known parameters and the imaginary susceptibility of the sample (χ_s''): $B_{F-s} = \frac{B_s S_s}{S_F}$

For an analytical solution, the magnetic circuit is solved. Starting from flux conservation in the contact surface between core and sample, $B_F = B_s$, and using the magnetomotive force (equation 2) to find the magnetic field in the circuit, it is finally found that $H_s = \frac{\mu_0 NI}{l_F}\frac{(1+\chi_F)}{5+\chi_F+4\chi_s}$, what leads to:

$$B_{F-s} = \frac{\mu_0 NI}{l_F}\frac{(1+\chi_s)(1+\chi_F)}{5+\chi_F+4\chi_s} \tag{5}$$

This result is obtained given the approximation $l_{a/s} = \frac{l_F}{4}$ and that the magnetic flux in the junction between the two U cores is twice the field produced in each one. In the opposite side (upper side according to Fig. 1) the magnetic induction (B_{F-a}) in the ferrite is directly related to the susceptibility of the air (approximated by that of the free space), and the magnetic $B_{F-a} = \frac{B_s S_s}{S_F}$ induction can be approached by:

$$B_{F-a} = \frac{\mu_0 NI}{l_F}\frac{(1+\chi_F)}{5+\chi_F} \tag{6}$$

Given that the susceptibility of the ferrite ($\chi_f = 2000$) is chosen to be > 6 orders of magnitude higher than the permeability of natural samples, we can assume that $B_{F-s} = B_{F-a}$. The phase (θ) induced in the electromotive force of the secondary coils in a differential acquisition can be considered as due to the break of the symmetry when the sample is approached (almost to contact) to the core and depends on the imaginary component of the complex susceptibility of the soil apart from other parameters.

2.2. Device

2.2.1. Sensor head

As it has been previously introduced, the susceptometer is based on an inductive circuit comprising an autoinduction with a ferrite H-shaped core and two capacitors connected in series and parallel with the coil (Fig. 1). The circuit is brought to the natural RLC resonance, which minimizes the power consumption.
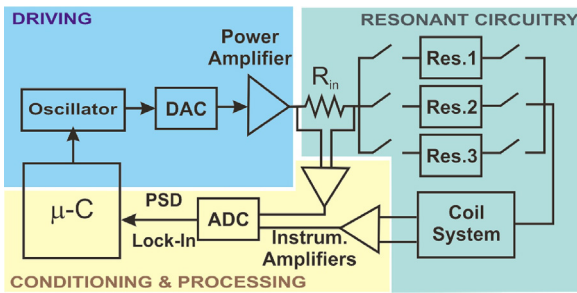
Fig. 3. Scheme of the autoinductance based on a U-shaped ferrite core.

Fig. 4. Set up for measurements indicating the main devices. The lock in oscillator is used for signal generation, the signal amplified is injected in the modified tank circuit and the readings are performed with the lock in amplifier by means of a PC code. The oscilloscope is only for user verification.

The autoinduction is composed by two U-shaped ferrite cores of envelope volume $25.8 \times 22.2 \times 16.0 \, mm^3$ (Fig. 2), with $d_1 = 6.6$, $d_2 = 16$, $h = 13$, $w = 19.2$. The winding is made with 15 turns of Litz wire to diminish losses. The permeability ($\mu_F = \mu'_F + i\mu''_F$) has been fitted to:

$\mu'_F (S.I.) = 2000$, practically constant in the frequency range between 10 and 100 kHz

$\mu''_F (S.I.) = 0.044f \, (Hz) + 7.55$, having a value of 10 ± 2 in the above-mentioned range,

which reproduces with an error < 1% the curve provided by the manufacturer.

The capacitors have been chosen of film type to surge the high current needed in the frequency range (10 and 100 kHz). In particular, they are of polypropylene foil, to minimize the internal ohmic losses and the parasitic inductance. It is foreseen a set of batteries of capacitors to tune the operation resonant frequencies of the circuit. Table 1 shows the values and main characteristics of C1 and C2 capacitors.

The prototype constructed with these elements has an efficiency in current between 1:06 and 1:37 (Table 1), achieving currents in the order of 10 and 20 A with an input current 1 A. These currents generate magnetic fields outside of the magnetic circuit in the order of 15/30 mT, which are considered enough to measure the susceptibility of the approached sample.

2.2.2. Proximity control electronic

The scheme of the electronics of a laboratory prototype is depicted in Fig. 3. The system is controlled by means of microcontroller (μC) MSP430F5438A-EP by Texas Instruments. The μC generates the signals to tune the frequency and selects the resonant circuit (Res. 1–3 in Fig. 3), controls the conditioning elements, acquires and processes the output signals.

Formerly, the μC performs a frequency sweep to tune the resonance of the selected circuit according to Table 1: 14.21, 31.42 or 56.80 kHz with controlled phase.

This is accomplished with an oscillator AD9833 by Analog Devices and by means of the instrumentation amplifier TLV5614 by Texas Instruments. A power amplifier is used to increase the current injected into the resonant circuit through R_{in} up to the above-mentioned level of 1 A approximately. The μC controls the magnitude of this current in a closed loop. Taking into account the gain factor of the circuit, this will establish a current in the branch of the coil of the resonant circuit according to Table 1, which will create the magnetic field in the ferrite gap.

The real and imaginary parts of the susceptibility are derived from the measurement of the resonant frequency shift and the phase variation of the induced field in the magnetic circuits when the sample is approached to the head. This is performed by means of a DSP lock in (implemented with an AD9833 oscillator and a DG211DJZ analogue switch) that receives the inputs through the instrumentation amplifiers and the analogue-to-digital converter (ADC) ADS1278 by Texas Instruments.
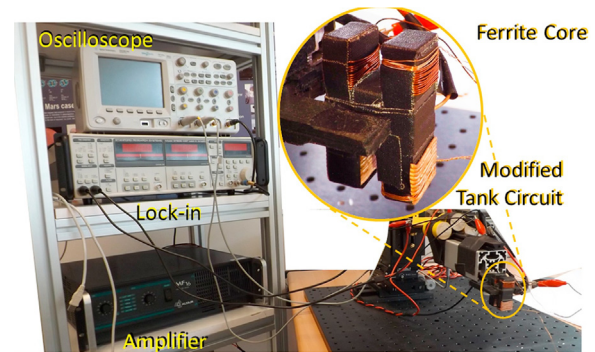
2.3. Operation

The complete set-up is presented in Fig. 4. The procedure to register a measurement is as follows:

Firstly, the system is tuned to one of its natural resonance frequencies, and the values of: this frequency, the phase of the electrical circuit and the phase of the secondary coils are acquired (reference values). Afterwards, the sensor head is approached to the sample. And the following parameters are acquired: the voltage drop through R_{in} (for refining purposes in the further calculations), the phase of the secondary coils and the differential field measurement between the part of the ferrite closed by the terrain (bottom part) and the open one (upper part). Afterwards, the system tunes the new frequency, which makes resonate the circuit, and this new frequency is acquired. Frequency sweep is used to determine χ' and the phase on the secondary coils is used to calculate χ" value.

The data given by the lock-in amplifier are processed to derive the two components of the susceptibility (χ' and χ") according to section II A. Then the system tunes the following resonant frequencies and repeats this same procedure.

3. Calibration

The calibration has been carried out by means of the use of a set of artificial samples with known compositions. The samples were made of a non-magnetic epoxy resin (ROYAPOX 511 by Royal Diamond) with a mass percentage content on magnetic material powder, i.e. iron (10 and 1 wt%), ferrite (1 wt%) or permalloy of composition Fe/Ni 19/81% (wt) by Metglas (1 wt%). The artificial samples, with a parallelepiped shape with average dimensions of $4 \times 3 \times 5$ cm ($60 \, cm^3$) were manufactured in the laboratory by using calculated composition of epoxy, hardener and magnetic material.

The sample preparation is as follows. The mixture preparation is poured in a handmade container with the above-mentioned shape made of polystyrene. In order to be able to remove the sample easily when the epoxy is cured, the inner walls of the container are coated with an aluminum foil and a thin layer of grease. Then the container is fixed to a rotatory system that spins at a period of 12 s for 24 h to achieve a proper homogenization of the magnetic powder in the epoxy volume preventing its deposition on the parallelepiped bottom base.

The results obtained for the imaginary part will be considered reference values for the measurements of unknown samples whilst the real part results will be calibrated against other equipment as follows:

Table 2
Results for Real Volume Susceptibility (χ') with different methods.

Sample (wt%)	VSM	FS (kHz)		PS (kHz)		
	DC	18	52,5	14,21	31,41	56,8
Fe/Ni (19/81) 1%	37 ± 2	37 ± 3	30 ± 4	30 ± 3	46 ± 3	35 ± 3
Ferrite 1%	33 ± 2	30 ± 3	26 ± 3	45 ± 3	38 ± 3	43 ± 3
Pure iron 1%	48 ± 4	54 ± 6	58 ± 5	43 ± 3	34 ± 3	45 ± 3
Pure iron 10%	444 ± 7	440 ± 50	430 ± 40	420 ± 30	400 ± 30	370 ± 30

Real Vol. Susceptibility (10^{-6} SI)

Table 3
Results for Imaginary Volume Susceptibility (χ'') with respect to the value of the Pure Iron 10% reference sample. These results have a common maximum uncertainty of 0.07 a.u.

Sample (wt%)	FS (kHz)		PS (kHz)		
	18	52,5	14,21	31,41	56,8
Fe/Ni (19/81) 1%	0.07	0.08	0.11	0.08	0.07
Ferrite 1%	0.05	0.05	0.12	0.10	0.08
Pure iron 1%	0.10	0.10	0.12	0.08	0.09
Pure iron 10%	$1\,(5,69 \cdot 10^{-5})$	$1\,(9,22 \cdot 10^{-5})$	$1\,(5,98 \cdot 10^{-2})$	$1\,(5,61 \cdot 10^{-2})$	$1\,(3,36 \cdot 10^{-2})$

Imaginary Vol. Susceptibility (a.u.)

The low-frequency calibration, which is considered equivalent to DC measurements has been made by comparison with a commercial equipment:

a) two VSM with electromagnet: one by LakeShore model 7304 at the Institute of Optoelectronics and Microelectronics Systems in the UPM, and another by ADE Magnetics model EV-7 at the Space Magnetism Laboratory, INTA.
b) a MS2E susceptometer by Bartington.

The higher frequency calibration (10 kHz–100 kHz) has been performed by comparison with Cobos et al. equipment "Cobos et al. [18]", designed to determine the magnetic losses on copper nanoparticles, modified and calibrated for this purpose. From now on we will refer Cobos et al. equipment as the fixed susceptometer (FS) and the presented device as the portable susceptometer (PS) referring to the fact that the former is part of the laboratory equipment and the latter is a handheld device.

This calibration consists in two steps. 1) A former calibration of the FS device by comparison of the 15 kHz measurements with a calibrated VSM (given that the losses at 15 kHz on permalloy Fe/Ni (19/81), ferrite and pure iron are negligible in comparison with the resolution of the device), and 2) the comparison of the measurements with the presented susceptometer and FS in their common frequency range.

Two of the frequencies selected for this FS prototype were almost the same as for the portable susceptometer, so that a direct comparison of the results for both devices can be done to prove reliability of the results and calibration. The results are shown in Fig. 5A and B, and presented in Tables 2 and 3.

The errors bars in Fig. 5A correspond to the uncertainty. This has been calculated as the maximum value of experimental and theoretical errors i.e. the experimental deviation respect to the reference techniques (VSM and FS), and the mathematical propagation of the error in the different contributions in equation 4.

The values of the imaginary component were normalized with respect to the sample with a 10% in iron powder content to avoid the measurement of the imaginary susceptibility in the relatively high range of frequencies, which is very complicated.

Despite of this, the inter-comparison of the different results for the different samples proves the capability of the instrument to measure relative values and their trend with frequency.

Results show sufficient resolution to distinguish materials and composition, high repeatability and high stability. Regarding the real part of the susceptibility, values of VSM and the PS are in very good concordance as it is shown in Fig. 5A. Regarding the imaginary part, the deviation between the PS and the FS responses, at the same frequencies, is attributed to the fact that the FS measures a very small portion of the samples (m $\sim$ 0.2 g and volume $\sim$ 8 mm^3) and the PS averages the susceptibility in a larger volume (volume $\sim$ 60 cm^3 i.e. 30·10^3 mm^3: 2 cm thickness, and 3 × 5 cm^2 surface). The size of the ferrite is directly related to the volume of action of the PS and this opens a field of numerous applications, as it will be discussed later in this work.

Despite the calibration materials have high susceptibility, their percentages are very low (between 1 and 10%), which means that the integrated susceptibility of the reference samples should be one tenth or one hundredth that of the materials susceptibility. This is fully representative of the range of natural rocks.

Regarding the imaginary part, the values show an analogue behavior of the values measured with the reference susceptometer (FS) but they are in the limit of resolution of the apparatus. This is also due to the fact that the expected values of the imaginary component of the reference samples are expected to be very low.

4. Results

The natural samples were supplied by the group of Paleomagnetism of the Earth, Astronomy and Astrophysics Department of the Complutense University of Madrid, and were chosen to cover a wide range of magnetic susceptibility: from a high susceptibility sample from a basalt dyke to an expected low susceptibility green clay, including an archeologic clay, and a representative sample of a terrace from Río Tinto terrestrial analogue of Mars.

In comparison with the results of calibration (with artificial and homogeneous samples), the results of the measurement of natural samples show identical repeatability and stability. It has been performed a classification in two groups: group 1 comprising VSM and FS, and group 2 comprising PS and MS2E corresponding to the different integration volumes of the sample: volume of group 1 in the order of 1 mm^3, and volume of group 3 orders of magnitude higher. This question has a more important influence in the case of samples with inhomogeneities, where a higher variability is shown in the results of Fig. 6A. This variability is particularly remarkable in the case of the peridotite, which is partially serpentinized giv-
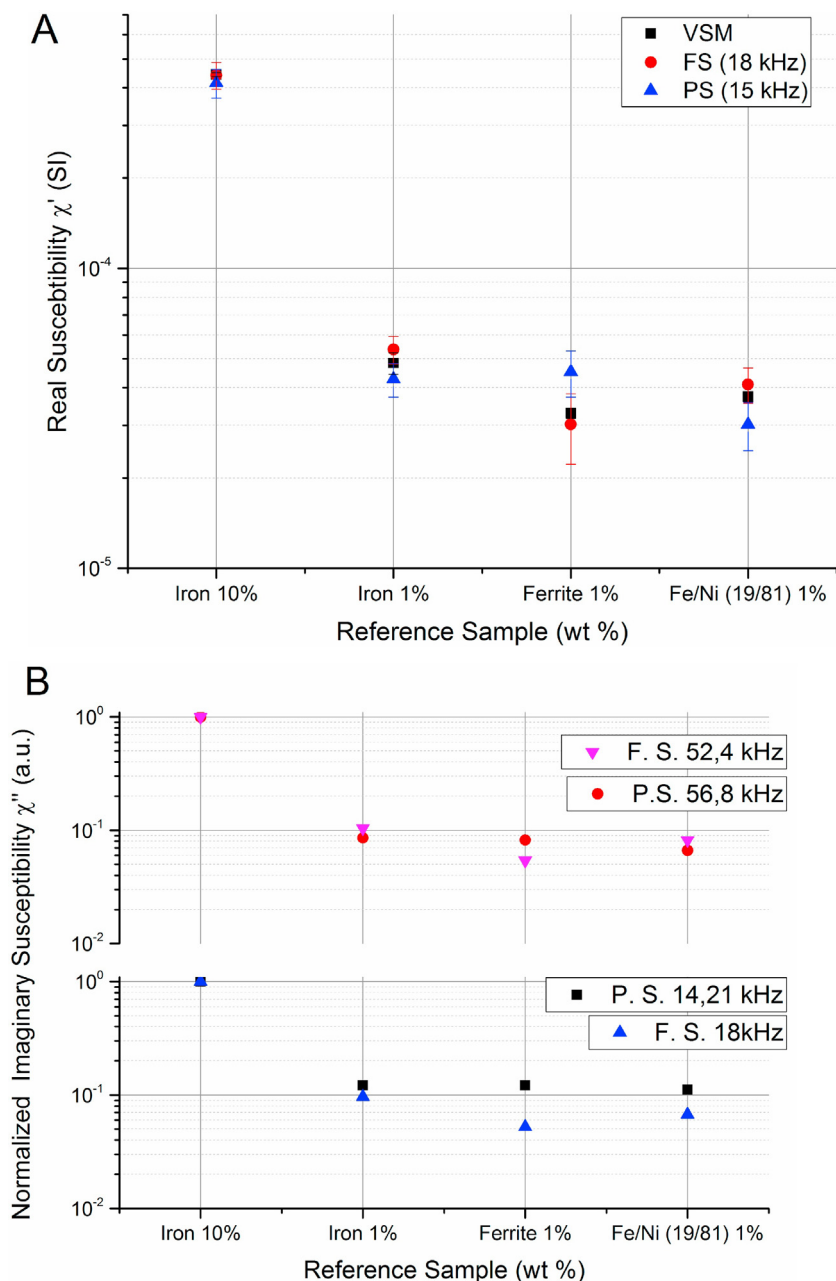
Fig. 5. A: Calibration of χ' vs. the reference samples. The different dots represent measurements with the different types of equipment at several frequencies, B: Stablishment of reference values of χ'' with respect to calibration sample Iron 10%. Figure shows the normalized values for the imaginary component of the susceptibility.The results are grouped together in the comparable frequencies for a better comparison. The uncertainty is estimated in 0.1 a.u.

Table 4
Results for Real Volume Susceptibility with different methods.

		Real Vol. Susceptibility (10^{-6} SI)
	VSM	*FS (kHz)*		*PS (kHz)*			*MS2E*
Sample (wt%)	*DC*	*18*	*52,5*	*14,21*	*31,41*	*56,8*	*2 kHz*
Basalt Dyke	15 ± 1	45 ± 2	65 ± 2	130 ± 30	108 ± 30	123 ± 30	107 ± 2
Peridotite (1)	...	...	...	775 ± 3	805 ± 3	844 ± 3	101 ± 2
Peridotite (2)	11 ± 1	12 ± 1	102 ± 3	54 ± 3	3 ± 3	3 ± 3	...
Red Clay	5 ± 1	7 ± 1	5 ± 1	9 ± 3	8 ± 3	3 ± 3	6 ± 2
Rio Tinto Terrace	1 ± 1	3 ± 1	1 ± 1	3 ± 3	3 ± 3	8 ± 3	2 ± 2
Green Clay	$0,8\pm1$	3 ± 1	...	3 ± 3	1 ± 3	8 ± 3	1 ± 2

ing rise to a two very different real susceptibility values in the area under test, named peridotite intrusion for the serpentinized area and peridotite (2) for not serpentinized area (Tables 4 and 5).

5. Discussion

The magnetic properties of natural samples are dominated by the presence of magnetic materials such as iron, nickel, etc. and
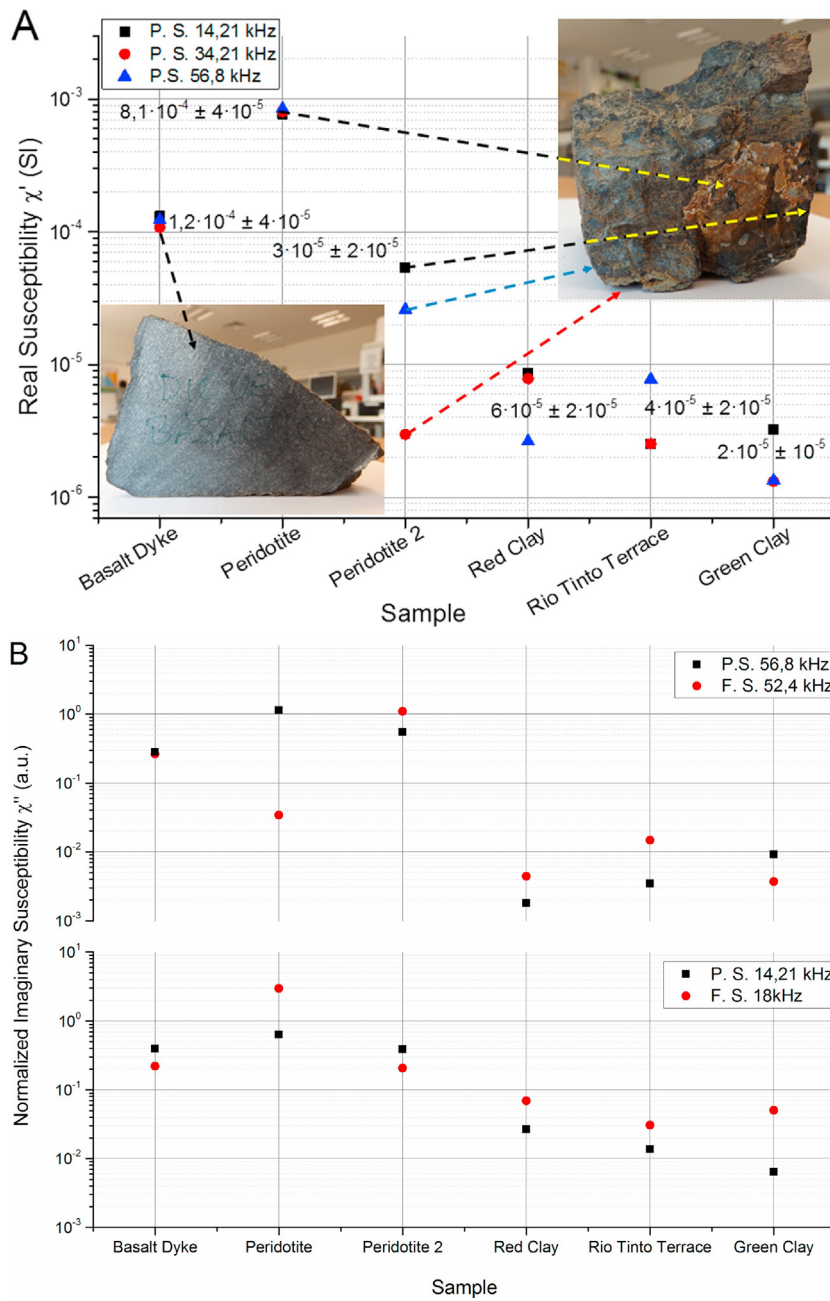
Fig. 6. A: Measurement of χ' of natural samples. The labels correspond to the averaged data of the measured frequencies. There are two results representations for the peridotite, given that this sample presents a intrussion of high susceptibility material. The inset images show the different surface distributions of two representative samples: the basalt dyke and the peridotite, where in can be distinguished the serpenized material intrussion B: Stablishment of χ" for the natural samples with respect to calibration samples. Figure shows the normalized values for the imaginary component of the susceptibility. The separeted graphics represent the results for imaginary component with the FS and PS at equivalent frequencies in arbitrary units.

Table 5
Results for Imaginary Volume Susceptibility (χ") with respect to the value of the Pure Iron 10% reference sample. These results have a common maximum uncertainty of 0.07 a.u.

	Imaginary Vol. Susceptibility (a.u.)				
	FS (kHz)		PS (kHz)		
Sample (wt%)	18	52,5	14,21	31,41	56,8
Basalt Dyke	0.22	0.26	0.39	0.27	0.28
Peridotite (1)	2.97	0.03	0.64	1.19	1.13
Peridotite (2)	0.21	1.10	0.39	0.08	0.55
Red Clay	0.07	0.004	0.03	0.02	0.002
Rio Tinto Terrace	0.03	0.01	0.01	0.01	0.003
Green Clay	0.05	0.004	0.01	0.003	0.01

the structure of the matter. The content in this materials and its domains structure can be delimited by determining magnetic properties such as saturation field, coercive field and magnetic permeability, and complemented with electrical information, i.e. permittivity and resistivity.

The proposed full device (vector magnetometer and susceptometer) measures the magnetic properties by analyzing them in a passive and in an active way, magnetizing the samples and collecting information of the state of magnetization. To directly determine the volume susceptibility, the device generates a magnetic field that penetrates in the soil and magnetize it, so the soil forms part of the magnetic circuit together with the ferrite core.

In the following some considerations are discussed:

• the geometrical approximations done in the calculations. With this respect, Fig. 7 sketches the model of the ferrite core (A), and the results of the magnetic models done with COMSOL (B and C).
• and the scope of the measurements in different scenarios.

Regarding the geometrical approximations, to calculate the volume or mass susceptibility, it is required either the volume or the mass of the magnetized sample. In the calculations several assumptions have been done affecting the sections where the magnetic field lines are confined in the different mediums, and the length of these lines.

One open question could be the hypothesis that $S_a = S_s$. Concerning this issue, extra simulations have been done using COMSOL software. In these simulations it is calculated the areas comprised by an isodynamic of 1 mT in the gap exposed to the air and in the gap closed by the soil. It has been found that the proportion between these two surfaces is in the order of 0.89, and therefore, the hypothesis has been considered as valid.

All the approximations are considered in the theoretical calculation of the error in the uncertainty values of the real component of the susceptibility mentioned in section II.

The other question concerning the geometry is the length of the magnetic circuit to have an estimation of the penetration depth into the soil. Fig. 7B shows the isolines distribution both in the air and in a sample with suscepbitilities between 10^{-6} and 10^{-3} (SI). At this point, the COMSOL simulation has identified the isodynamic of 1 mT (Fig. 7C), and it has been done a plot of this line in the magnetic circuit. This plot has been fitted with Origin to calculate the path numerically. This permits to do the line-integral of the field. This analysis has been used to validate the assumption that the length of the magnetic circuit through the air/soil is 1/4 of the length of the circuit in the ferrite.

The other question concerning the site of prospection is linked to this last question. Since the penetration depth is limited to < 1 cm, in many sites this susceptibility measurement would cast data of the soil which covers the rocks and would not be able to provide information on the rocks. This restricts the areas of application to sites where the rocks are outcropped and not covered by vegetation or a soil.

Under the above mentioned constraints, a device combining magnetic field and susceptibility measurements is very useful for the high-resolution magnetic surveys in the context of the Earth prospections and the planetary exploration, very important in the next decade "Michelena and Kilian [13]; Díaz-Michelena et al. [19]; Michelena and Kilian [13]" highlight that one of the limitations to derive conclusions of the surveys is the lack of an in situ measurement of the susceptibility. This extra measurement can be of high importance because it permits the in situ determination of the Koningsberger ratios and with high values of these rations one can use the in situ measurements to constrain properties of the global fields during the rocks formation. Also the determination of the susceptibility plays an important role in the identification of iron-rich
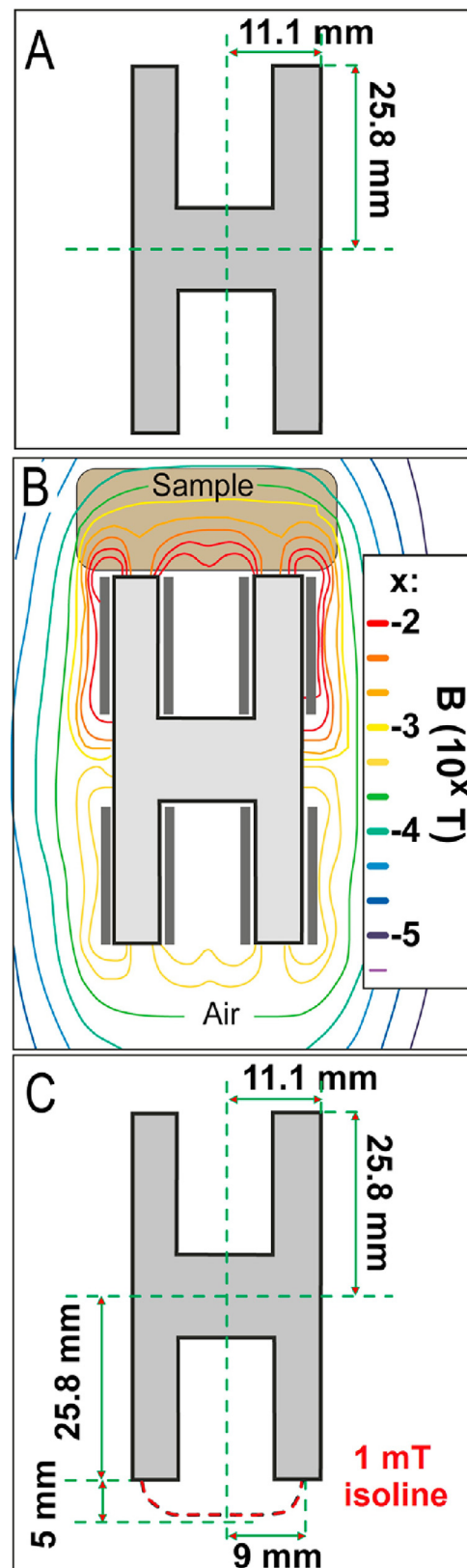

Fig. 7. A. 2D Model of the ferrite core, B. Illustration of the magnetic isolines in the air and sample gaps, C. Sample ($10^{-6} < \chi < 10^{-3}$) penetration depth for 1 mT isoline. The calculations have been performed with COMSOL and adapted to the illustration.

minerals and their alteration processes as well as their structures in single, multi or pseudo single domain structures. Therefore, the inclusion of such multisensor device (magnetometer + susceptometer) in a suit of instruments including spectrometers can be of key importance in the search of the tiny clues which can evidence extraterrestrial life. Together with the vector magnetometer, the ability of this device to induce magnetization would also make the dual device capable to sketch minor hysteresis cycles of the soils and rocks.

Future improvements of this instrument are focused on the widening of its capability to perform Anhysteretic and Isothermal Remanent Magnetization measurements (ARM and IRM). In order to achieve this, the current gain ratios in the circuit needs to be improved and a system to include a DC field with the used of batteries of capacitors is being studied.

6. Conclusions

The described instrument is a novel portable device to measure the magnetic complex susceptibility of rocks and other samples in situ without the need to load the sample in a system. The whole instrument has two boxes: one sensor head and an electronic box with masses of 200 and 250 g, volumes of $60 \times 60 \times 50\,mm^3$ and $60 \times 60 \times 40\,mm^3$ respectively, and a power consumption < 6 W.

The easiness of use makes it a very good choice for Earth prospections and planetary exploration.

The combination of the instrument with a vector magnetometer can be clue in the exploration of terrains where the access is complicated, and its combination with geological modules in rover can make a huge step forward in the planetary exploration.

This device aims to complement current state of the art techniques in field campaigns on Earth and planetary exploration, and also intends to become a low cost, reliable, robust, and low maintenance cost device for laboratories that cannot host SQUID devices or large and high cost laboratory equipment to measure the complex magnetic susceptibility.

Acknowledgments

References

[1] R. Singh, R. Lal, U.C. Upreti, D.K. Suri, A.V. Narlikar, V.P.S. Awana, J. Albino Aguiar, Md. Shahabuddin, Superconductivity in Zn-doped tetragonal laBaCaCu3O7-δsystems, Phys. Rev. B 55 (1997) 1216–1222.

[2] C.A.M. Mulder, A.J. van Duyneveldt, J.A. Mydosh, Susceptibility of the CuMn spin-glass: frequency and field dependences, Phys. Rev. B 23 (1981) 1384–1396.

[3] E.D. Barco, N. Vernier, J.M. Hernandez, J. Tejada, E.M. Chudnovsky, E. Molins, G. Bellessa, Quantum coherence in Fe8 molecular nanomagnets, EPL (Europhys. Lett.) 47 (1999) 722.

[4] K. Pandarinath, R. Shankar, I.S. Torres-Alvarado, A.K. Warrier, Magnetic Susceptibility of volcanic rocks in geothermal areas: application potential in geothermal exploration studies for identification of rocks and zones of hydrothermal alteration, Arab. J. Geosci. 7 (2014) 2851–2860.

[5] P. Marcon, K. Ostanina, Overview of methods for magnetic susceptibility measurement, PIERS Proceedings, Kuala Lumpur, Malaysia March 27–30 (2012).

[6] S. Foner, Versatile and sensitive vibrating-Sample magnetometer, Rev. Sci. Instrum. 30 (1957) 548–557.

[7] G. Asti, M. Solzi, P. Podini, Phase and frequency control in the vibrating wire magnetic susceptometer, Sens. Actuators A 81 (2000) 343–345.

[8] M. Motta, F. Colauto, R. Zadorosny, T.H. Johansen, R.B. Dinner, M.G. Blamire, G.W. Ataklti, V.V. Moshchalkov, A.V. Silhanek, W.A. Ortiz, Visualizing the ac magnetic susceptibility of superconducting films via magneto-optical imaging, Phys. Rev. B 84 (2011) 214529.

[9] S. Li, D. Hurt, M. Toth, B. McElfresh, A. Amann, S. Spagna, A low background magneto-Optic probe for high, Sens. SQUID Susceptometer. IEEE Trans. Mag. 50 (11) (2014) 2504704.

[10] D. Drung, J.-H. Storm, F. Ruede, A. Kirste, M. Regin, T. Schurig, A.M. Repollés, J. Sesé, F. Luis, Thin-Film Microsusceptometer with integrated nanoloop, IEEE Trans. Appl. Supercond. 24 (4) (2014) 1600206.

[11] J. Duyn, MR susceptibility imaging, J. Magn. Reson. 229 (2013) 198–207.

[12] V.P. Timofeev, C.G. Kim, V.I. Shnyrkov, Susceptometry application of portable HTS SQUID-Based system, J. Mag. 3 (3) (1998) 86–88.

[13] M. Díaz Michelena, R. Kilian, 'Magnetic signatures of the orogenic crust of the Patagonian Andes with implication for planetary exploration', Phys. Earth Planet. Inter. 248 (2015) 35–54.

[14] A. Clark, Seeing Beneath the Soil, 1990 (Batsford London).

[15] K.J. Murdock, K. Wilkie, L. Brown, Rock magnetic properties, magnetic susceptibility, and organic geochemistry comparison in core LZ1029-7 Lake El'gygytgyn, Russia Far East, Clim. Past. 9 (2013) 467–479.

[16] R. Day, M. Fuller, V.A. Schmidt, Hysteresis properties of titano-magnetites: grain-size and compositional dependence, Phys. Earth Planet. Inter. 13 (4) (1977) 260–267.

[17] D.J. Dunlop, Theory and application of the Day plot (Mrs/Ms ver-sus Hcr/Hc) 1. Theoretical curves and tests using titanomagnetite data, J. geophys. Res. 107 (B3) (2002) 2056–2071.

[18] P. Cobos, M. Maicas, M. Sanz, C. Aroca, High resolution system for nanoparticles hyperthermia efficiency evaluation, IEEE Trans. Mag. 47 (10) (2011) 2360–2363.

[19] M. Díaz-Michelena, R. Kilian, R. Sanz, F. Rios, O. Baeza, Mars MOURA magnetometer demonstration for high-resolution mapping on terrestrial analogues, Geosci. Instrum. Methods Data Syst. 5 (2016) 127–142.

Biographies

Marina Díaz Michelena PhD in Physics from Polytechnic University of Madrid (2004). Current position: head of the Space Magnetism Laboratory at the Spanish National Institute or Aerospace Technology (INTA).Dr. Díaz Michelena has evolved a line in miniaturized and compact magnetometers for space and planetary applications. The magnetometers in Earth orbit are currently being used for Space weather purposes. As a result of this development activity she has grown an interest in planetary magnetometry. In particular devoted to develop new instruments for Mars and Moon magnetic mineralogy as well as in the investigation of terrestrial analogs.

José Luis Mesa Uña PhD Student at the Spanish National Institute or Aerospace Technology (INTA).José Luis Mesa Uña finished his MSc in Physics in the Autónoma University of Madrid (2012) and is currently doing his PhD in devices devoted to the measurement of the magnetic susceptibility. The main area of application is the planetary exploration.

Marina Pérez Jiménez PhD Student at the Institute of Optoelectronic Systems and Microtechnology (ISOM).Marina Pérez Jiménez finished his MSc in Telecommunication Engineering in the Polytechnic University of Madrid (2013) and is currently doing her PhD in highly specialised magnetometric devices.

César Marco Maicas Ramos PhD in Physics from Complutense University of Madrid (1996). Current position: Titular professor on the ETSIST, UPM Madrid. Researcher at the Institute of Optoelectronic Systems and Microtechnology (ISOM).Dr. Maicas is a specialist in magnetic simulation comprising finite and boundary elements method. Presently he is collaborating in several projects of different nature from spintronics to instrumentation for planetary exploration.

Pedro Cobos Arribas PhD in Telecommunication Engineering from Polytechnic University of Madrid (2001). Current position: Titular professor on the ETSIST, UPM Madrid. Researcher at the Institute of Optoelectronic Systems and Microtechnology (ISOM).Dr. Cobos Arribas did his first research work with a fluxgate application, as his Final year Proyect, in 1990. He is currently involved in the design and development of microcontroller circuits solutions for magnetic applications, as linear motor controllers, magnetic detectors and magnetic detection instruments.

Claudio Aroca Hernández-Ros PhD in Physics from the Complutense University of Madrid (1980). Current position: Prof. Dr. Head of the Department of Physics Applied to the Information Technologies Department of the Polytechnic University of Madrid. Subdirector of the Institute of Optoelectronic Systems and Microtechnology (ISOM). Prof. Dr. Aroca started his research in the study of magnetic structures in amorphous magnetic materials. This research derived in an applied activity in the field of magnetic sensors and instrumentation. At ISOM he has focused on thin film materials study, the exchange interaction in these systems, and development of planar sensors. He is currently involved in the design and development of spintronic based devices and in the study of magnetic nanoparticles and its application for biomedical technologies as NMR contrast and MEG.